Titan's Induced magnetosphere from plasma wave, magnetic field and particle observations

R. Modolo[1], N. Romanelli[2,3], C. Bertucci[4], J.-J. Berthelier[1], P. Canu[5], R. Piberne[5], A.J. Coates[6], F. Leblanc[1], N. J. T. Edberg[7], M. Morooka[7], M. Holmberg[8], E. Dubinin [9], L. Regoli [10], W.S. Kurth[11], D.A. Gurnett[11], J.-E. Wahlund[7], H. Waite[12]and M.K. Dougherty[13]

[1]LATMOS / UVSQ / SU / CNRS, 11 bd d'Alembert, 78280 Guyancourt, France
[2]NASA Goddard Space Flight Center, Greenbelt, Maryland, USA
[3]CRESST II, University of Maryland, Baltimore County, USA
[4]Institute for Astronomy and Space Physics - IAFE, Ciudad Universiteria, Buenos-Aires, Argentina
[5]LPP-Ecole Polytechnique, 91128 Palaiseau Cedex, France
[6]MSSL University College London, Holmbury St Mary, Dorking RH5 6NT, UK
[7]IRF, Box 537, SE-75121 Uppsala, Sweden
[8]European Space Agency - ESTEC, 1 Kepleeran, Noordwijk, The Netherlands
[9] Max Planck Institute, MPS, Gottingen, Germany
[10]Johns Hopkins University Applied Physics Laboratory, Laurel, Maryland, USA
[11]The Univeristy of Iowa, Dept of Physics and Astronomy, Iowa City, USA
[12]Southwest Research Institute, San Antonio, Texas, USA
[13]Imperial College of Science, Technology and Medicine, Space and Atmospheric Physics Group, Department of Physics, London SW7 2BW, UK

Key Points:

- We analyze Titan's induced magnetosphere making use of CASSINI RPWS, CAPS and MAG measurements from 82 flybys
- We derive the first global electron density map of Titan's near environment, that ranges between 10^{-2} to 10^{3} cm^{-3}, delimiting an average induced magnetosphere standoff distance of 1.85 R_T and 2.77 R_T on the ram and flank direction respectively.

Corresponding author: Ronan Modolo, ronan.modolo@latmos.ipsl.fr

- We identified ionospheric ions with energies between 10 eV to 3 keV, increasing along the convective electric field direction, with an intensity of 0.7 mV/m, consistent with an average estimate of 0.61 mV/m deduced from $|\vec{v}\times\vec{B}|$ calculation.

Abstract

Cassini plasma wave and charged particle observations are combined with magnetometer measurements to investigate Titan's induced magnetosphere. Electric field emissions close to Titan are identified as upper hybrid resonance emissions, which provide a density estimate of Titan's cold plasma. These observations have been combined with electron spectrometer measurements to build an integrated map of electron density in Titan's near environment using observations from TA to T82 flybys, *ie* which includes flybys from the Cassini prime, equinox and part of the soltice mission. We identify a dense ionospheric region and an extended plasma wake with values ranging between 10^{-2} and 10^{3} cm^{-3}. Upstream of the induced magnetosphere, the presence of pickup ions in the positive hemisphere of the kronian plasma convective electric field are detected. The mass of the observed pickup corresponds to methane group ions, N_2^+ and $HCNH^+$ ions as well as Titan's protons and molecular hydrogen ions. These ions are progressively accelerated by the kronian background electric field and we estimate its intensity by reconstructing the energization of this population. We find values on the order of 0.7 mV/m , consistent with an average estimate of 0.61 mV/m deduced from $\sim |\vec{V} \times \vec{B}|$ computation.

1 Introduction

Titan's interaction with the ambient plasma in Saturn's magnetosphere has been categorized as atmospheric, like the ones for Mars, Venus and comets with the solar wind (Barabash, 2012). Titan's atmosphere is partly ionized, leading to the formation of an ionosphere, which acts as an obstacle against the magnetospheric plasma flow. This conductive obstacle deflects the incoming flow and twists the magnetic field around the body and leading to a draped field line region, mostly populated by ionospheric or exospheric plasma, called the induced magnetosphere, as illustrated by Waite et al. (2004, Figure 7). Reviews on Titan's ionosphere, composition and its induced magnetosphere have been presented in Cravens et al. (2010) and Wahlund et al. (2014).

Cassini has revealed a highly variable and dynamic upstream plasma environment largely influenced by the complex nature of Saturn's magnetosphere and its magnetodisk (Arridge, Achilleos, & Guio, 2011; Arridge, André, Bertucci, et al., 2011; Arridge, André, McAndrews, et al., 2011; Arridge, 2012). As a result, efforts on the characterization and categorization of the upstream plasma properties of the magnetic field (Bertucci et al.,

2009; Simon et al., 2013), electron distribution function (Rymer et al., 2009) and plasma density variation (Morooka et al., 2009) have been carried out. Indeed, Bertucci et al. (2009) have shown that the magnetic field at the orbit of Titan has a large variability and is affected by several factors, such as the presence of Saturn's magnetodisk. Consequently, Titan is exposed to different magnetic orientations going from North-South to planetward field lines, to highly perturbed fields, when Titan is inside Saturn's current sheet. Large fluctuations of the magnetospheric configuration are commonly observed between the inbound and outbound portions of passes, that occur over periods of a few minutes up to several hours, and thus affect the external draping of the magnetic field lines around Titan (Simon et al., 2010). While (Edberg et al., 2015) have presented ionospheric density map, below 2400 km, based on Langmuir Probe obervations, a characterization of the electron density inside Titan's magnetosphere is thus of interest.

Pickup ions have been observed in the vicinity of various bodies in the Solar System such as comets, Mars, Titan, Moon, Enceladus (e.g., Coates et al., 1989, 1993; Dubinin et al., 1993, 2006; Hartle et al., 2006; Yokota et al., 2009; Tokar et al., 2008). At Titan, pickup ions have been observed by Voyager 1 (Hartle et al., 1982) and Cassini (e.g., Hartle et al., 2006). These ions have large masses around 16 amu or more and arise from the ionization of Titan's upper atmosphere and they are embedded in the magnetospheric flow. When picked-up by the magnetospheric flow they are accelerated by the motional electric field $\vec{E} = -\vec{v} \times \vec{B}$, where $\vec{v}$ is the plasma bulk velocity and $\vec{B}$ the local magnetic field, providing an ion escape mechanism responsible for the erosion of Titan's atmosphere.

In this work we further characterize this unique environment making use of Magnetometer (MAG) measurements (Dougherty et al., 2004), particle data (CAPS) (Young et al., 2004) and Radio and Plasma Wave Science (RPWS) observations (Gurnett et al., 2004), providing an overall and organized description of the electron plasma environment of Titan and the pickup ion distribution. Based on such results, we also estimate the convective electric field intensity responsible for such ion population. In section 2, we introduce the approach to combine both particle and wave data to build a continuous electron density profile for each flyby of Cassini prime, equinox and the beginning of the solstice mission. The global image of the electron density in the near region of Titan is presented and discussed in section 3. Section 4 is dedicated to the description of the pickup ion population through its energy signature, mass composition and its organization with

respect to the ambient electric field. A discussion on the energization of these pickup ions completes this section while section 5 summarizes the main conclusions of this work.

2 Measurements and methodology

RPWS observations can be used to measure the electron number density of the thermal plasma close to Titan. Information derived from these wave electric fields data and from Langmuir probe (LP) provide two independent density estimates for the cold plasma. This study we have mainly used electron number density derived from waves emissions. Electrostatic emissions have been detected in the range from 1 to several hundreds of kHz. The most intense and structured emissions occur at the upper hybrid frequency, $f_{UH} = \sqrt{f_c^2 + f_p^2}$, with f_p the plasma frequency and f_c the electron cyclotron frequency. In Titan's vicinity, given the relatively weak magnetic field strength, the electron cyclotron frequency is much smaller than the electron plasma frequency ($f_c \ll f_p$), so the upper hybrid frequency is essentially equal to the electron plasma frequency and f_{UH} provides a direct visualization of electron density profiles. Most of the Titan flybys exhibit f_{UH} signatures either on the Medium Frequency Receiver (MFR) or on the High Frequency Receiver (HFR) and electron densities estimated by this method are in excellent agreement with previoulsy published LP data (Edberg et al., 2010).

Electron Spectrometer observations of the Cassini Plasma Spectrometer (CAPS-ELS) are used to compute the electron number density in Saturn's magnetosphere and Titan's environment. CAPS-ELS measures suprathermal electrons distribution in the energy range from 0.6 eV to 28 keV with an energy resolution of 17% and an angular resolution of 20°. Moments, and particularly the density, are determined based on the work of Lewis et al. (2008).

CAPS-ELS moment calculation underestimate electron density in the cold plasma region since only part of the electron distribution function is seen due to a negative spacecraft potential and also due to a relatively coarse energy discretization table below 1eV. On the other hand, f_{UH} signatures are not observed below 1-5 kHz (corresponding to 0.01-0.3 cm^{-3}). While the particle instrument is well designed for hot and tenuous plasma, the wave instrument is very well adapted to measured cold and dense plasma The excellent complementarity of the two data set is illustrated in Figure 1.

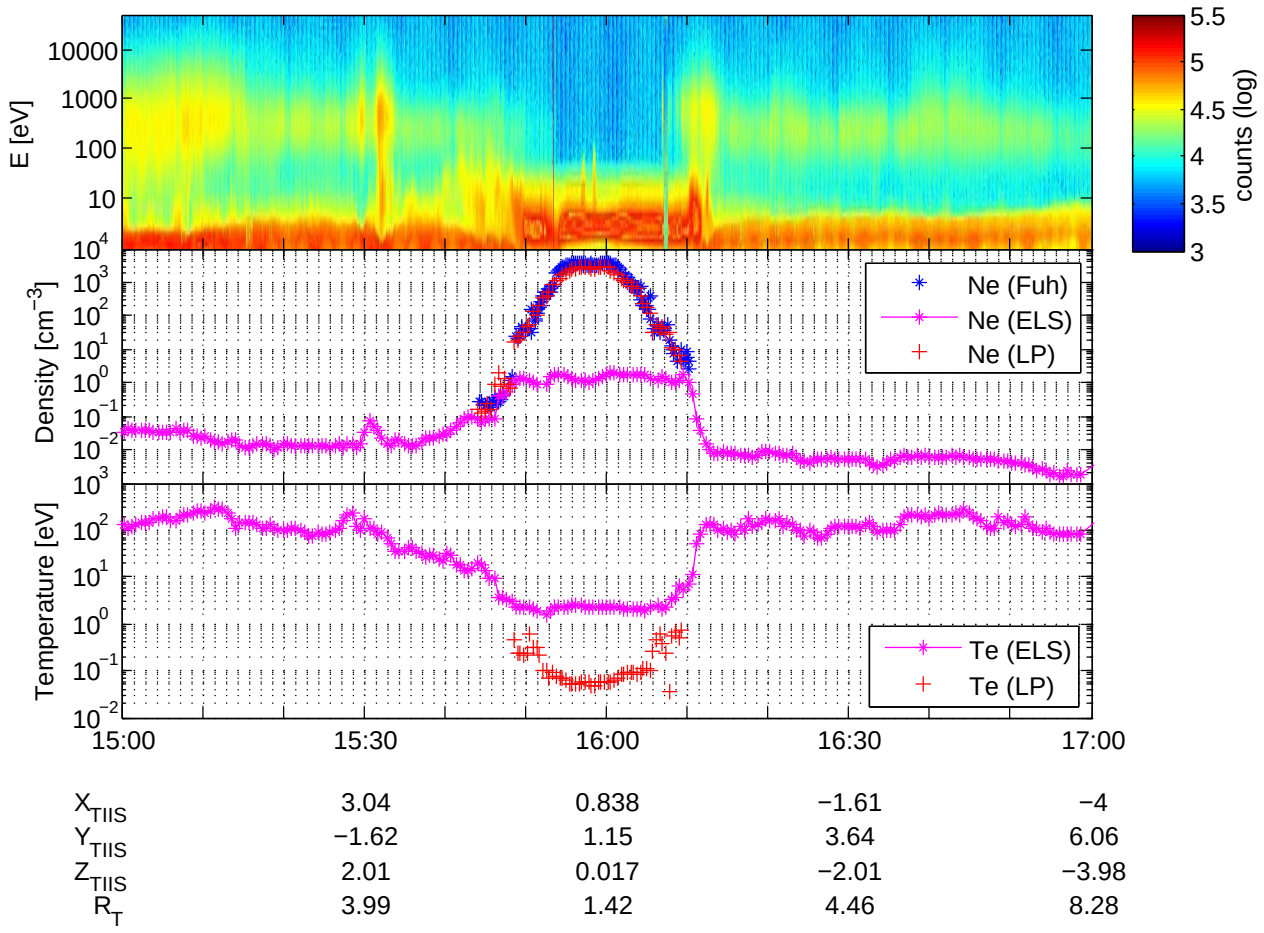

Figure 1. CAPS-ELS and RPWS observations for T20 flyby (2006 /10/25). Top panel shows CAPS-ELS Anode 5 observations. Middle panel presents electron number density estimated by CAPS-ELS moment calculation (magenta marks), LP analysis (red marks) and deduced from wave observations (blue marks). Bottom panel shows electron temperarture estimated by ELS (magenta marks) and LP analysis (red marks).

Figure 1 shows electron density and temperature profiles retrieved from different techniques and instruments for the T20 flyby (2006/10/25). We present data in the Titan interaction coordinate system (TIIS) where the positive X-axis is defined by the direction of the ideal co-rotational kronian plasma flow and the Y-axis points toward Saturn. The Z-axis completes the right handed coordinate system.

everal regions with different plasma regimes are crossed during this Cassini flyby. The spacecraft is first located in Saturn's magnetosphere, characterized by a density range of 0.01-0.1 cm^{-3} and an electron temperature of $\sim$ 100 eV. As Cassini approaches Titan's ionized environment, the electron number density progressively increases, while the electron temperature decreases. Titan's ionosphere is clearly identified by a high electron density, a low electron temperature and the signature of ionospheric photoelectrons in the CAPS-ELS spectra (Coates, 2009). In the ionospheric region, the electron density deduced from LP data and f_{UH} are almost identical. The closest approach occured at an altitude of 949 km at 15:51 SCET. The outbound leg is relatively symmetric to the inbound one, both in terms of regions crossed and global plasma parameter trends.

On all flybys analyzed (up to T82), a good correspondance between the density estimated from CAPS-ELS and RPWS is observed most of the time between 0.1 - 1 cm^{-3} density interval, as illustrated in figure 1. When both RPWS and CAPS-ELS measurements were present during the same time interval, RPWS measurements were systematically prefered sincethey provide directly the electron density through the plasma frequency.

MAG observations are used to derive information about the background magnetic field environment in the vicinity of Titan, to quantify its variability and also to emphasize the bipolar tail region reported by Simon et al. (2014).

CAPS-IMS observations have also been used to derive information on the ion population, in particular the mass composition of the plasma for specific time intervals (see section 4.2). CAPS-IMS samples ions in 8 angular sectors each of them having an identical field of view (FOV) of $8° \times 20°$. "Singles" data correspond to energy-per-charge (E/Q) spectra ranging from 1eV to 50 keV with a spectral resolution of 17%. The electrostatic analyzer is scanned 8 sweeps, each 4.0 s long and with 64-step energy steps, referred as a A-cycle lasting 32.0 s. CAPS-ELS and IMS sensors are mounted on a rotating platform capable of sweeping the CAPS instrument by $\sim 180°$ around an axis par-

allel to the spacecraft Z-axis in about 3 min 30s. The Time-Of-Flight (TOF) analyzer is used to infer detailed compositional analysis in a so called B-cycle. During the B-cycle, the 8 angular sectors are summed together and the 64 energy steps are collapsed to 32 energy steps. The B-cycle lasts 256 s. More detailed information of CAPS-IMS are presented in Young et al. (2004); Hartle et al. (2006); Sittler et al. (2010).

3 Electron density maps

CAPS-ELS and RPWS electron density estimates are combined to provide a unique and continuous electron density profile going from Saturn's magnetosphere to Titan's ionosphere, for each flyby. All flybys from TA to T82 have been analyzed with the exception of T7 / T73, T9 and T32, for which no data have been recorded, or a significant deviation from the ideal co-rotation flow has been emphasized (e.g., Szego et al., 2007) or the flyby occurred in Saturn's magnetosheath. In each case, the upper hybrid line has been digitalized with the ViTos vizualization tool which display the MFR/HDR spectrum for each acquisition. On each wave spectrum, the ViTos tool proposes the frequency of maximum wave intensity; we have confirmed the selected frequency, or we have reselected manually a new frequency, as the f_{UH} emission frequency. Only data with a clear upper hybrid signature have been retained. Two consecutive spectra are separated by about 7 s for the low rate data. A relatively smooth density profile, similar for the wave and the LP data set, is seen when the spacecraft enters or leaves Titan's induced magnetosphere. As illustrated in Figure 1, between about 15:45 UT and 16:10 UT and emphasizes a good level of confidence on the electron density measurements.

Figure 2-a presents the overall density map in Titan's environment deduced from these combined data sets. This map corresponds to the mean values of the electron density sampled up to the T82 flyby. The mean values have been calculated by binning the data on a spatial grid where the abscissa is aligned with the TIIS X-axis and the ordinate is defined by $\rho_{TIIS} = \sqrt{Y_{TIIS}^2 + Z_{TIIS}^2}$. Cylindrical symmetry with respect to the TIIS X-axis is therefore assumed. The bin size used is 0.155 R_T (400 km), where R_T = 2575 km is the radius of the Titan. Figure 2-b shows the map of the standard deviation of the electron density and Figure 2-c illustrates the sampled regions with th number of bins covered in our study.

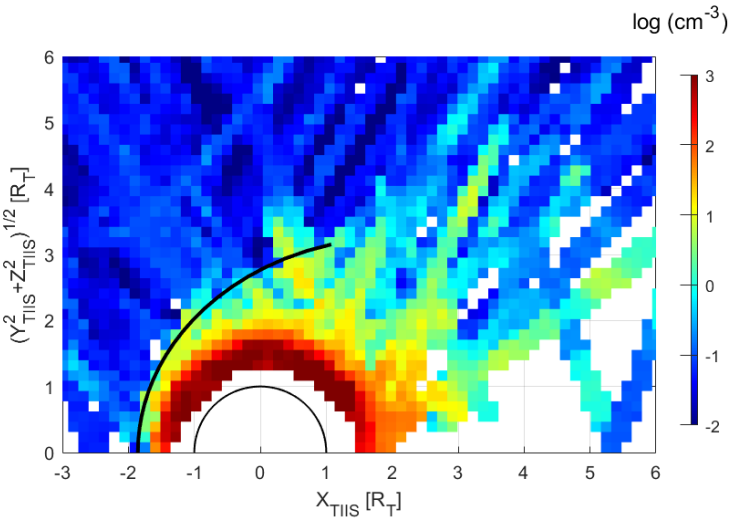

a-

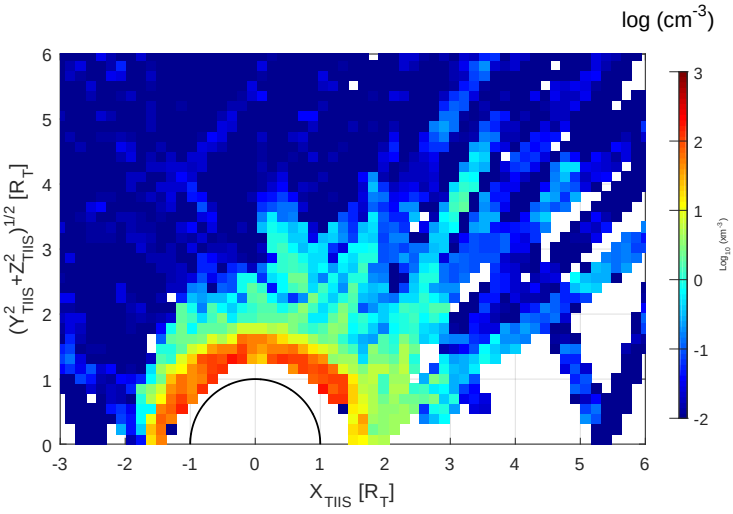

b-

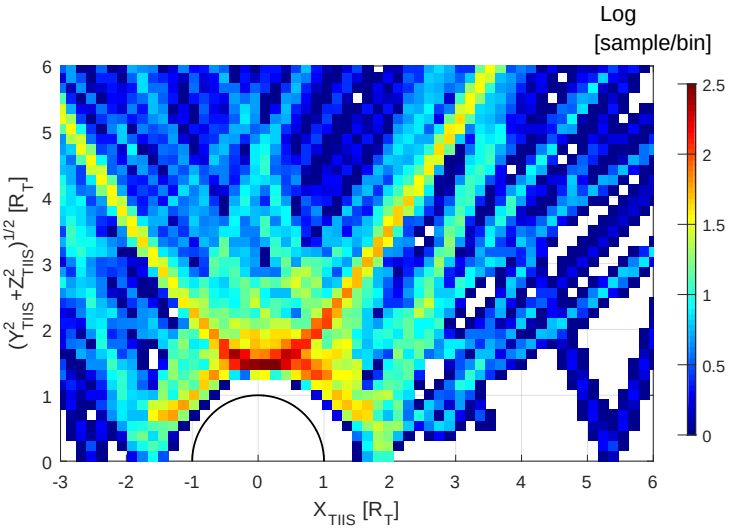

c-

Figure 2. a- Global electron density map in a cylindrical frame centered on Titan deduced from combined RPWS and ELS observations from TA to T82. The black elliptic line indicates the location of the induced magnetosphere (cf text) b- Standard deviation map of electron number density. c- Cassini coverage for the TA-T82 flybys

Figure 2 includes all analyzed flybys, regardless of the external conditions. Therefore the presented electron density map includes varioussolar illumination conditions, upstream plasma flow (electron density distribution, density and possibly composition), magnetic field orientation (dipolar, planetward or swept-back fields). These different upstream conditions have been emphasized by Bertucci et al. (2009); Garnier et al. (2010); Rymer et al. (2009); Simon et al. (2010); Németh et al. (2011); Edberg et al. (2013); Regoli et al. (2018). Edberg et al. (2015) have carefully addressed the influence of Saturn's magnetosphere on Titan's ionosphere, they also have shown that the dayside ionosphere is significantly denser than the nightside. Variation in these parameters affect Titan's induced magnetosphere and contribute to blur the electron number density map. The resulting variability of the electron density is reflected in the standard deviation map (Figure 2-b). The bin size, 400 km, might also contibute to increase the standard deviation value inside the density map bin since its spatial size is larger than the ionospheric scale height. Based on these maps, the characteristics of the plasma in the Titan environment can be summarized as follows. Firstly we observe a good statistical sampling of the ionospheric region. Globally, a reasonable sampling was achieved for the induced magnetosphere with more than 10 samples (from several flybys) in each bin with no statistical bias in the electron density map. Figure 2-a reveals a dense ionospheric region, with values larger than 1000 electron cm^{-3}, with a relatively large standard deviation of several hundreds of electron cm^{-3} (Figure 2-b). This result is consistent with previous studies (e.g., Ågren et al., 2009; Edberg et al., 2010). The induced magnetosphere boundary separates Saturn's magnetospheric plasma from Titan's ionospheric plasma. As seen in figure 1, a sharp change on the density profile is usually observed. The induced magnetosphere can be roughly identified at locations where the electron number density is larger than 1 cm^{-3}, since Saturn's magnetospheric plasma do not reach such density value at Titan's orbit (?, ?). Similar location of Titan's induced magnetospheric boundary can be derived from the gradient of the density profiles. A more accurate location of the induced magnetosphere might require to include criteria on the magnetic field and plasma flow observations.

In order to delimit the external envelop of the induced magnetosphere, we have fitted in the ram side and the near wake region, up to $X_{TIIS} = 1$ R_T, the 1 cm^{-3} isocontour with a function corresponding to an ellipse. Expressed in polar coordinates, assuming a symmetry along the X_{TIIS} axis, the equation of the induced magnetosphere

surface is $r = \frac{L}{1+\epsilon\cos\theta}$ where the polar coordinate (r, θ) are measured about the focus X_0, L is the semi-major axis and ϵ is the eccentricity. The fitted conic parameters are $X_0 = 0.25$ R$_T$, $L = 2.52$ R$_T$ and $\epsilon = 0.57$. We did not extend the fit calculation in the middle and far Titan's wake because of the limited coverage. The fit of the induced magnetosphere boundary is represented by the black curve in figure 2-a. A conic function has also been used to delimit the induced magnetosphere or magnetic pile-up boundary for Mars and Venus (and references therein Bertucci et al., 2011). Chen and Simon (2020) have shown that the magnetic pile-up boundary present some asymmetry in the Saturn facing/ anti-facing side due to the gyromotion of the pickup ions , emphasizing the limitation of the cylindrical symmetry assumption. Such asymmetry in the direction of the motional electric field has been also observed for the Martian induced magnetosphere (Halekas et al., 2017; Dubinin et al., 2019).

Although figure 2-a does not show plasma composition, it suggests than Titan's planetary plasma can reach several tens of cm^{-3} at about 3 R$_T$ and several cm^{-3} at about 6 R$_T$ in the tail region. The induced magnetospheric boundary is closer to the planet on the ram side than on the flank side and the plasma scale height is much larger in the wake than on the ram side. From the induced magnetosphere fit, two parameters have been determined : R_{SD} which is the ellipse stand-off distance along the X_{TIIS} axis and R_{TD} which is the ellipse stand-off distance along the ρ_{TIIS} axis. We found $R_{SD} = 1.85$ R$_T$ and $R_{TD} = 2.77$ R$_T$. Simulation results are also consistent with this global electron density map (e.g., Ledvina et al., 2012; Ma et al., 2006; Modolo & Chanteur, 2008; Sillanpää et al., 2006; Simon et al., 2007; Snowden et al., 2007).

The lack of coverage in the center of the far tail ($R > 3R_T$ and $\rho < 1R_T$) and the use of a cylindrical representation, does not allow a clear distinction of the two ionospheric separated tail structures identified in a few flybys (Coates et al., 2012). Nevertheless such a graphic provides an upper limit of the cross-section tail area at different distances in the tail, assuming a cylindrical symmetry, which might be useful to compute the ionospheric loss rate. For instance Coates et al. (2012) assumed an area of πR_T^2 to compute the escape rate, similiar to Modolo et al. (2007). According to Figure 2-b, the area of this disk might have been underestimated. A more detailed determination of the plasma loss rate is beyond the scope of this paper. The reader is referred to Wahlund et al. (2005), Coates et al. (2007), Szego et al. (2007), Modolo et al. (2007), Sittler et al.

(2010), Edberg et al. (2011), Coates et al. (2012), Westlake et al. (2012) and Romanelli et al. (2014), for some case studies of plasma loss rates estimates.

4 Pick-up ions observations

Ions from a planetary origin can be produced upstream of the induced magnetosphere. These ions, incorporated into the background plasma flow, are so-called pick-up ions. They are accelerated by the motional electric field $\vec{E} = -\vec{v}\times\vec{B}$, moving in a plane perpendicular to B. Theoretical investigations and global hybrid simulation modeling have emphasized the asymmetry between the $+\vec{E}$ and $-\vec{E}$ hemispheres for pickup ions (Hartle et al., 2006; Modolo & Chanteur, 2008). The large gyroradii of the pickup ions have been also suggested to cause an asymmetry between Titan's Saturn facing and adverted hemispheres on the magnetic pile-up profiles (Chen & Simon, 2020). In addition, due to their large gyroradius compared to the neutral scale height, pickup ions appear as narrow beams in velocity space (Hartle et al., 2006; Hartle & Sittler, 2007; Hartle et al., 2011).

The detection and characterization of ion cyclotron waves is another approach to identify the presence of pickup ions, as has been done for Mars or Venus (e.g., Romanelli et al., 2013; Delva et al., 2012). While direct measurements have identified this population at Titan from the ion mass spectrometer data, ion cyclotron waves are rarely observed at Titan in magnetic field data (Russell et al., 2016). An explanation, Cowee et al. (2010) suggested that the growth time is too long compared to the convection time of background plasma through the interaction region so that the ion cyclotron waves have not enough time to grow to amplitudes that can be observed by the Cassini magnetometer. Therefore data from the ion mass spectrometer remain the only and most direct way to study the pick-up ion population in Titan's vicinity.

Regoli et al. (2016) have performed a survey of pickup up ions and found their presence in the anti-Saturn side which leads to conclude that CAPS-IMS have captured freshly produced pickup ions. In this paper, we go one step further by organizing the pick-up ion observations in a reference frame depending of the magnetic field and characterizing their progressive acceleration.

4.1 Pickup ion identification through their energy signature

Pick-up ions signatures were searched in the CAPS-IMS data over the full set of T0a-T82 flybys. As examples, we found such signature at the edge of Titan's induced magnetosphere in flybys TA, T06, T39 and T42. Other flybys exhibit similar signatures. Figure 3 displays their energy characteristics and their location in 4 sets (a,b,c,d) corresponding to the four mentioned flybys, each with 2 panels. The bottom panels of each set show Cassini trajectories drawn in cylindrical TIIS coordinates, while top panel displays the average flux measured by the 8 anodes of CAPS-IMS. Patchy and repetitive structures observed in the magnetospheric region are due to the actuator motion of the platform hosting the particle instruments.

We clearly see the progressive deceleration of the incoming plasma on the inbound and outbound legs of each of these flybys and the entry of Cassini into Titan's ionosphere as indicated by low energy signatures (<100 eV) and high particle counts. The narrow beam energy signatures, indicated by the black arrows, suggest that these features arise from the detection of pickup ions. For these specific observations, the angle between the background magnetic field and the bulk plasma flow ranges between 70° and 140°. The observed ion pickup energy is smaller than the theoretical expected maximum, given by $4m_{pi}/m_{am}E_{am}\sin^2\theta_{vB}$ where m_{pi}/m_{am} is the ratio between ion pickup mass and the ambient ion mass, E_{am} is the energy of the ambient plasma, and θ_{vB} is the angle between the ambient plasma flow velocity and the background magnetic field direction.

The location of the observed events are reported on the Cassini trajectory with black circle symbols. These events occur in the external part of the induced magnetosphere, usually near one of its flank, or in the kronian plasma region. This finding is consistent with global simulation results which reported pickup ions with relatively high energy in the flank of the induced magnetosphere, and more precisely in the +E hemisphere accoriding to simulation results and theroretical expectations (e.g., Modolo & Chanteur, 2008, their Figure 7).

The narrow beam signature in energy and velocity space is illustratred in Figure 4. It shows the angular distribution of the plasma between 01:12 and 01:14 SCET at the energy bin 25 (E=788 eV) for the T63 flyby, in the Saturn Solar Ecliptic (SSE) coordinate system (Figure 4-a). In this coordinate system the X_{SSE} points towards the Sun, the Z_{SSE} is perpendicular to ecliptic plane, in the northern celestial hemisphere, and the

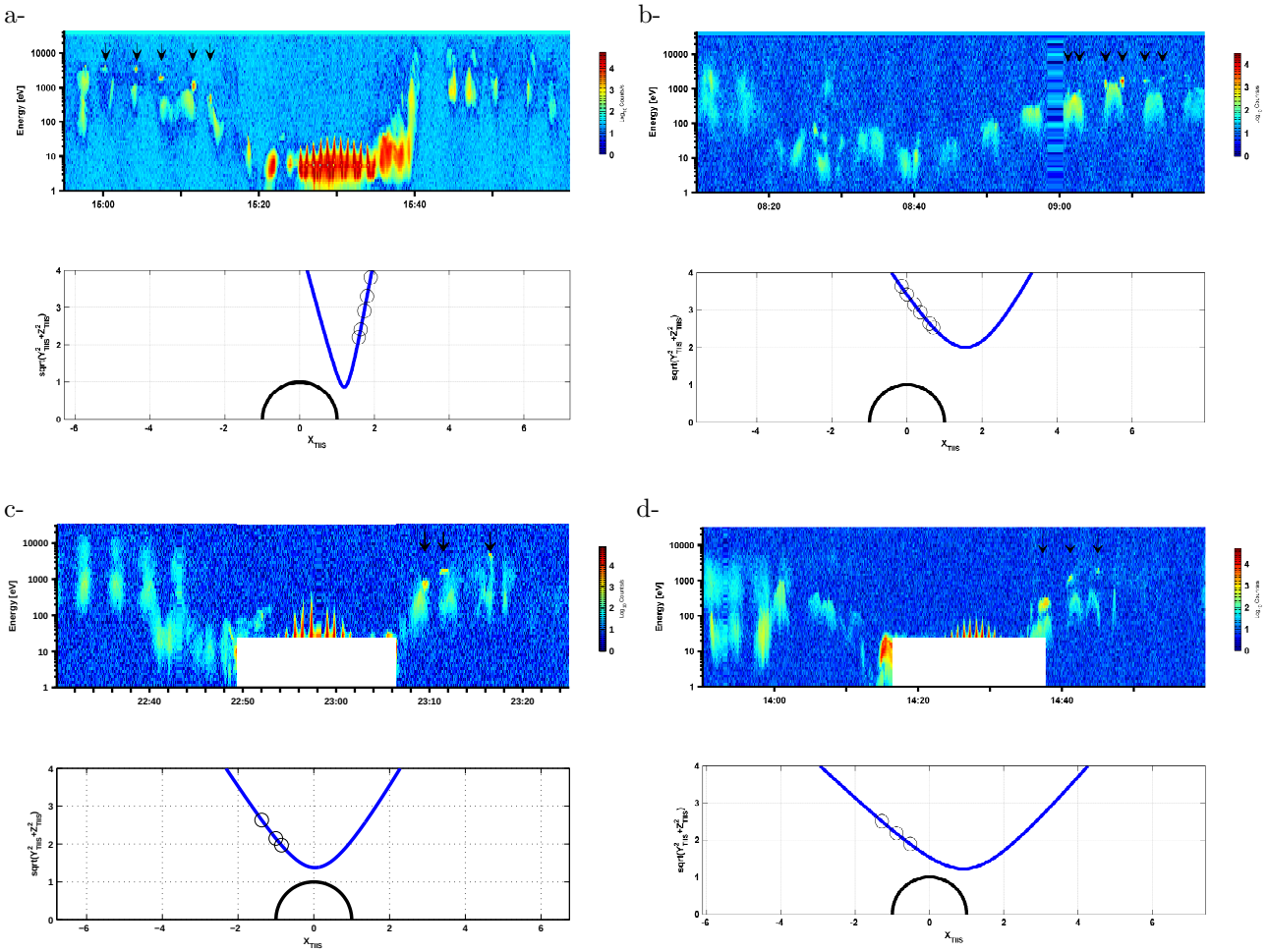

Figure 3. 4 set of figures (a,b,c,d) displaying the trajectory and CAPS-IMS observations for flybys TA, T06, T39 and T42, respectively. Each set has a top panel presenting CAPS-IMS observations and a bottom panel illustrating Cassini trajectory (blue line) for the corresponding flyby in cylindrical TIIS coordinate system. Black arrows in the CAPS-IMS panels indicate the presence of pickup ions. Their locations are reported on Cassini trajectory with a circle mark. The energy table change on CAPS-IMS near closest approach produces the white rectangles displayed on panels c and d.

Y_{SSE} completes the right hand system. The field of view of CAPS-IMS during this 2 min time interval covers only a small part of the full-sky. We can see an increase of counts/s in a very localized area pointing toward $-Y_{SSE}$, corresponding to the pickup ions. The instrument is therefore capturing ions moving away from Saturn, consistent with the expected electric field direction and the cartoon of Titan's environment illustrated in Waite et al. (2004).

Figure 4-b displays, in polar (r, θ) coordinates, the energy-pitch angle distribution for the same time interval. The magnetic field measurements have been averaged during the 2 min interval. The r coordinate represents the energy in a logarithmic scale, from 1 eV to 46 keV, while the θ coordinate indicates the pitch angle. The $\pm x$ direction of the plot implies a parallel / anti-parallel direction (with respect to the local magnetic field) and the y direction means a direction perpendicular to the magnetic field. Pickup ions are seen with a pitch angle close to 90° and with an energy slightly lower than 1 keV. Another example of energy - picth angle and angular distribution is presented for the T70 flyby in Figure 4-c and d, and similar conclusions are reached.

4.2 Pickup ion mass composition

Hartle et al. (2006) reported on pickup ion composition for the TA flyby. TOF analysis suggested the presence of H^+, H_2^+, N^+/CH_2^+, CH_4^+ and N_2^+ with possible contribution of CH_3^+, CH_5^+, $HCNH^+$ and $C_2H_5^+$. The ion mass composition during flyby T39 (TOF acquisition from 23:11:48 to 23:16:04 SCET) indicates the presence of pickup ions reported next. Figure 5 displays the counts of the Straight Through (ST) detector as a function of energy per charge versus time of flight channel.

When ions enter through the CAPS-IMS sensor they first pass trough the electrostatic analyzer (ESA) which allow the determination of the energy per charge of the particle. This information is presented on the y-axis of figure 5. At the exit of the ESA, particles are pre-accelerated and impact a carbon foil, emitting secondary electrons. These electrons are attracted by the positive $\sim 15kV$ potential and hit the the ST detector giving the start signal of the TOF for the mass identification. When atomic or molecular species pass through the carbon foil they are break up in more elementary particles (neutral particles, postively or negatively charged ions). Neutral atoms and negatively charged particles travel through the TOF chamber and hit the ST detector, pro-

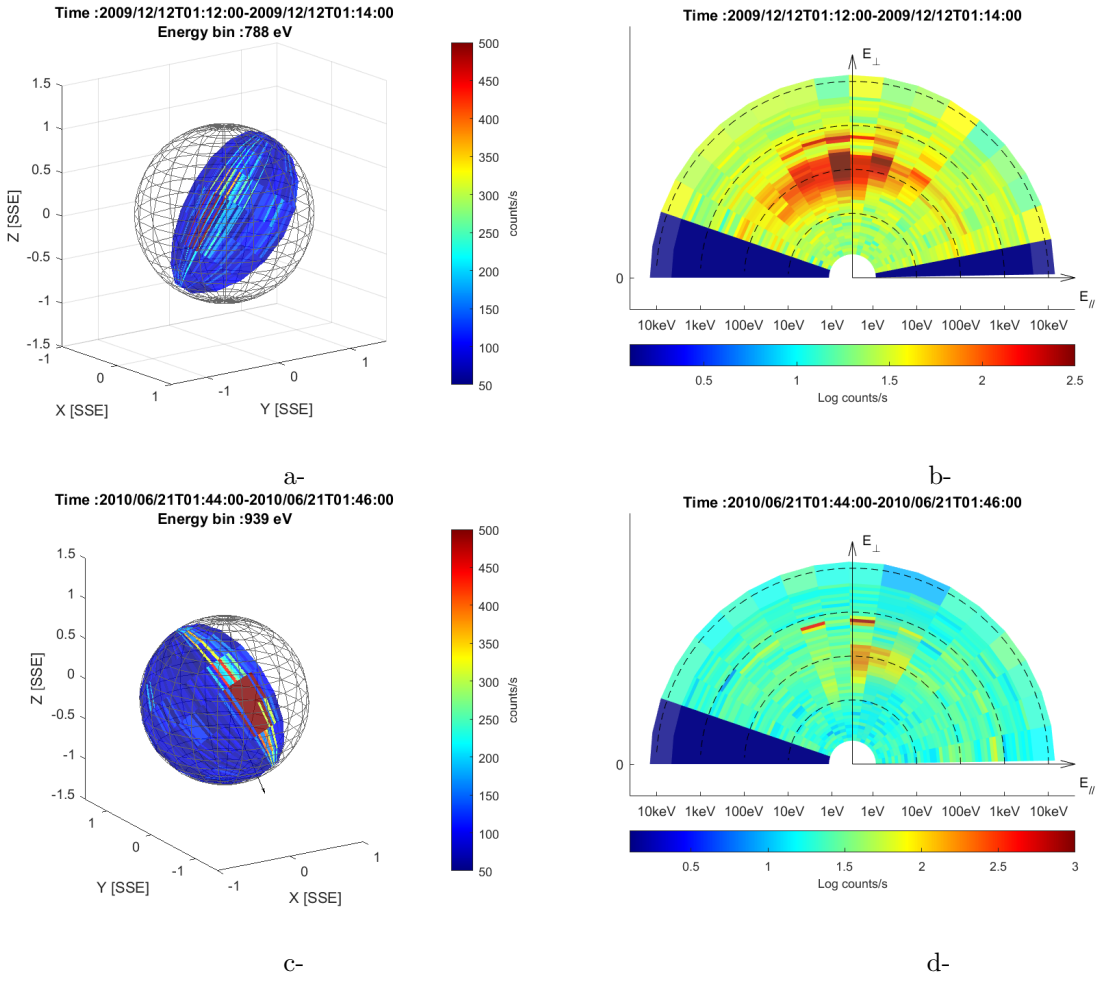

Figure 4. Panels a and c show the angular distribution during the T63 and T70 flyby respectively in the SSE coordinate system. Pickup ions have been indentified at time 01:12-01:14 SCET and at the energy 788 eV for the 63 flyby and at time 01:44-01:46 SCET at the energy 939 eV for the T70 flyby. Panel b and d display energy - pitch angle distribution in polar coordinate.

ducing a stop signal. The difference of time between the start and the stop signals determine the time of flight and is presented on the x-axis of figure 5. For a given energy per charge, lighter species will have shorter time of flight than heavier species and will be identified at smaller TOF channels. A more detailed description of the CAPS IMS intsrument and the mass identification can be found in Young et al. (2004), Wilson et al. (2012) and Thomsen et al. (2014).

In this B-cycle (Figure 5) , the ion energies range from about 10 eV to few keV and there is a mixture of ambient and pick-up ions. Figure presents a mixture of ambient and pickup ions. Thomsen et al. (2010), and Wilson et al. (2017) have presented ion moments at Titan's orbit indicating that H^+, W^+ (water group ions) and H_2^+ compose to the magnetopsheric plasma. On the other hand, Felici et al. (2018) have suggested that Titan could also be a source of H_2^+ ions due to a maximum ratio of H_2^+/H^+ near Titan's orbit. For ions below 1 keV, the compositional analysis reveals H^+ and H_2^+ ions. The ambient plasma differs from the pick-up ion population not only from their energy signature but also from their incoming flow direction. The low energy species present a different angular distribution compare to the 1 keV species, indicating different flow directions and therefore suggesting distinct populations.

At about 1 keV, the spectrogram indicates heavier species. These ion species with an energy slightly above 1 keV correspond to the IMS energy pickup ion identification presented at Figure 3-c (first black arrow). By filtering TOF data in the energy range 1-3 keV, one can thus determine the mass composition of the pick-up ion alone.

A simulation model, developed by Nelson and Berthelier (2009), characterizing the IMS instrumental response to various ion compositions at different energy, has been used to interpret the TOF signatures as accurately as possible. Simulation results have been compared to test chamber calibration measurements for several ion masses (atomic and molecular species with mass ranging from 12 to 28 amu) and at different energies (from 1024 eV to 27560 eV). The simulation model is able to reproduce most of the observed IMS calibrated ST and LEF (Linear Electric Field) measurements for a specific ion species at a given energy.

A library of ST and LEF signatures for several atomic and molecular species with different energies has been built. By considering different compositions for this plasma we are able to compare the ion-summed simulated signatures with the measurements.

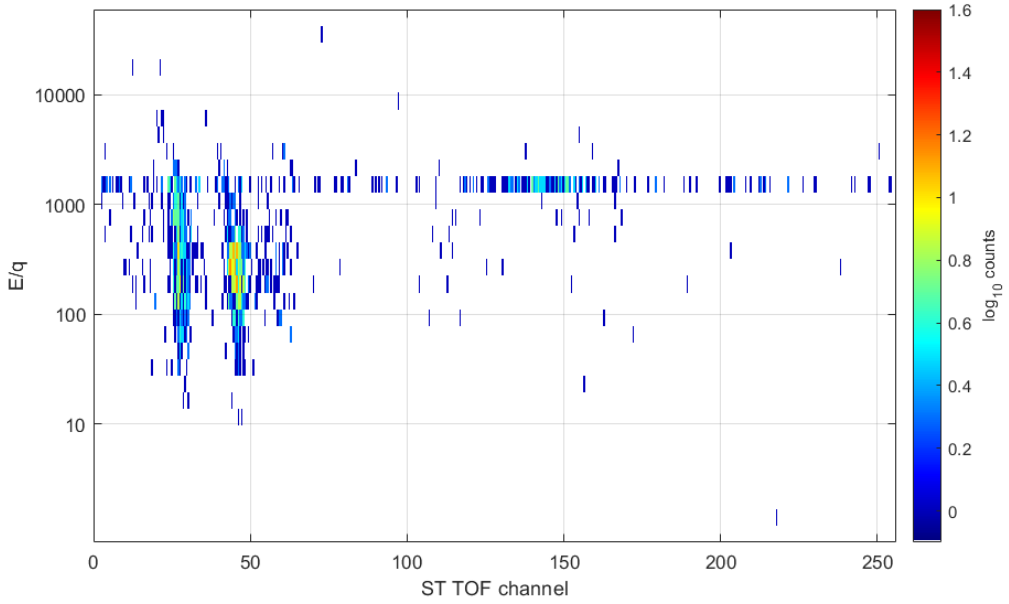

Figure 5. IMS-TOF spectrogram of the ST detector for the T39 flyby acquired at ∼23:11 SCET. Counts, color coded with a logarithmic scale, on the ST detector are plotted as energy per charge (E/q [eV]) versus TOF channels.

Figure 6 top panel presents simulated results of several ion species at ∼ 1keV (H^+, H_2^+, CH_3^+, $HCNH^+$ and N_2^+). Figure 6 bottom panel displays a comparison between simulated result and TOF observations. From the simulated results, three main patterns on the ST are expected for CH_3^+ (green curve) ions at 1keV, according to the simulation model. The main CH_3^+ peak located around TOF bin 150, contributing to the peak identified by label (2) in the bootom panel, is produced by a start signal issued by an electron and a stop signal from a neutral carbon atom. The second CH_3^+ peak at TOF bin 100 corresponds to the case of a start generated by an electron and stop generated by a negatively charged carbon ion C^-. A more diffuse contribution around TOF bin 50, identified as the label (3) in the bottom panel, is believed to be due to a start time initiated by an electron and a stop time of a secondary electron ejected from high voltage rings after an impact of neutral carbon or hydrogen atom. Each species has its own signature on the ST and LEF. As can be seen in Figure 6, it is impossible to dissociate the contribution from $HCNH^+$ (yellow) from N_2^+ (magenta) at this energy on the ST. The two curves are superimposed at TOF bins 190-240 and are expected to be due to a start/stop time infered by an electron and neutral nitrogen and carbon atoms, produc-

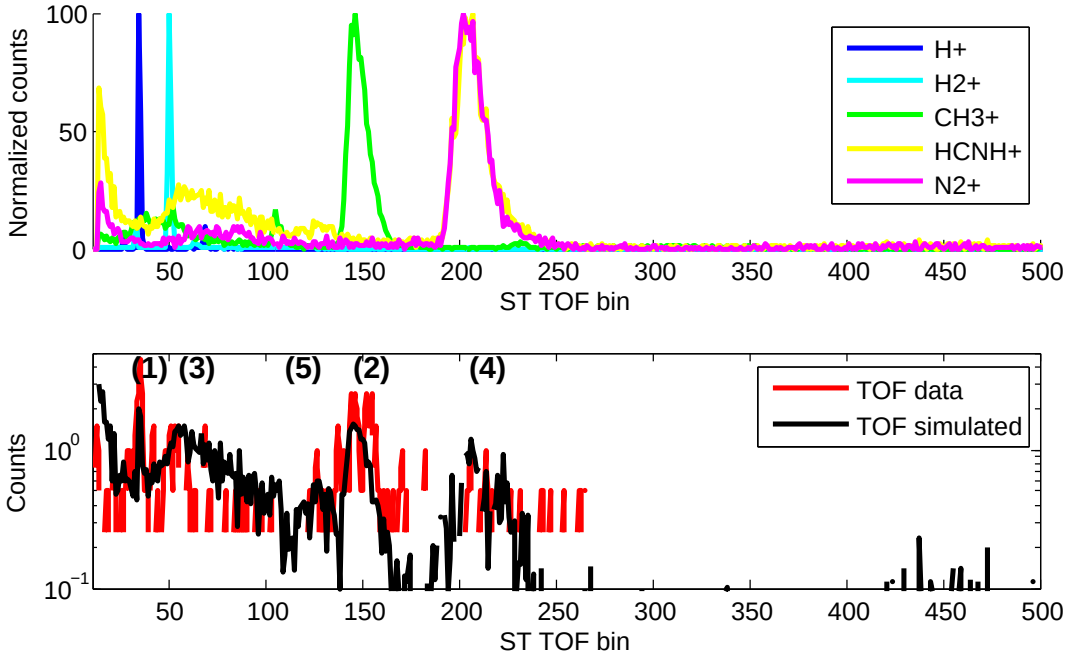

Figure 6. Simulated ST signatures for ion species at about 1keV (H^+, H_2^+, CH_3^+, N_2^+ and $HCNH^+$) are presented on the top panel while the bottom planel displays a comparison between ST IMS-TOF counts and simulated results. ST observations have been acquired at ∼23:11 SCET during the T39 flyby.

ing the relatively large peak label (4) in the simulation/observation comparison panel. Due to the small pick-up ion flux, no significant count rates on the LEF helps thus preventing to distiguish between these 2 different species. Peaks label (1) and (5) in the bottom panel correspond to a start/stop time due to an electron and a neutral hydrogen in the first case and an electron and c^- and N^- in the second case. The overall signatures thus indicate that the ion population near the flank of the induced magnetosphere is mainly composed of H^+, CH_3^+, $HCNH^+$ or N_2^+. Thus, this pickup composition for flyby T39 is similar to the TA observations (Hartle et al., 2006).

Unfortunately TOF measurements by CAPS-IMS do not always allow determining the mass composition due to insufficient number of counts on the LEF and ST detectors. Nevertheless, when available, TOF measurements present signatures similar to those shown in Figure 6 and suggesting the presence of the methane group (CH_2^+, CH_3^+, CH_4^+, CH_5^+) as well as of heavier species such as H_2CN^+ or N_2^+. The column 7 of Table 1 summarizes the information on the mass composition of picku ions when a mass identifications of the pick-up ions was possible.

4.3 Pickup location and energization

The characteristicse of pickup ions are intrinsically related to the motional electric field and magnetic field directions. Bertucci et al. (2009) and Simon et al. (2010) have shown that the magnetic field at Titan is highly variable and only few of the flybys gives an ambient field matching the Voyager 1 conditions. Therefore the geographical TIIS coordinate system is not the most appropriate, and a draping coordinate system based on the incoming flow and magnetic field direction is expected to better describe, organize and help in the interpretation of the formation of the induced magnetosphere. In this draping system, the X_{DRAP} axis is aligned with the corotational flow direction, the Z_{DRAP} axis points in the opposite direction of $\overrightarrow{B_{z_{DRAP}}} = \overrightarrow{B_{y_{TIIS}}} + \overrightarrow{B_{z_{TIIS}}}$ and Y_{DRAP} completes the right handed system. Such a coordinate system is similar to the DRAP system suggested by Neubauer et al. (2006), except that a non-zero Bx_{DRAP} component is allowed, affecting the location of Titan's neutral sheet.

Bertucci et al. (2009) have shown that the Saturn magnetodisk strongly affects Titan's upstream magnetic environment and exposes the moon to either dipolar-like fields close to SLT 12h and planetward, or sweptback fields in the midnight, dawn and dusk

sectors. To derive meaningful average ambient magnetic fields, it is important to infer time scales for Titan's interaction. Based on one study by Bertucci et al. (2008), so called fossil magnetic field lines have been observed in Titan's ionosphere. They provide information about the "age" of draped magnetospheric field lines and their convection time in the ionosphere. Lifetimes of these field lines are expected to range between 20 min to 3 hours. This time interval corresponds to the time for a magnetospheric magnetic flux tube to reach Titan's deep ionosphere (1000-1200 km altitude).

In our study the ambient magnetic field is averaged during a 30 min period inbound and a 30 min period outbound of each flyby. The time intervals used to compute the average values have been taken such that the spacecraft is located outside of the region with draped field lines around Titan. Since our study focuses on the external part of the induced magnetosphere, short time intervals close to Titan's induced magnetosphere are favored over larger intervals while the deep ionosphere will take a longer time to be affected by the upstream conditions.Magnetic field averages used for this study are, sometimes, slightly different from those suggested by Simon et al. (2010) who averaged over longer time intervals (about 3 hours inbound and 3 hours outbound). Table 1 reports a synthesis of information on the flybys analyzed showing a signature of Titan's induced magnetosphere. Each flyby is identified by its denomination, the date and time of its closest approach. The location of Titan with respect to Saturn is indicated in the Saturn Local Time (SLT) column and shows that all configurations are covered, although the pick-up ion region might not be explored for all local times. The average ambient magnetic field inbound and outbound in the TIIS coordinate, as well as the presence of pick-up ion signatures determined from their energy characteristic and composition by CAPS/IMS are reported in the respective columns.

To compute the draped coordinate system, we assumed a linear dependance between the inbound and outbound magnetic field values. The draped coordinate system is therefore computed for the time of each flyby and observations are represented in this changing reference frame. When the determination of an average ambient field (inbound or outbound) is impossible, either due to large variations in the kronian plasma or the difficulty to determine accurately when the spacecraft is located in kronian plasma region, we assumed that the ambient field is constant during the whole flyby. In the cases where both inbound and outbound average magnetic field could not be determined, results are displayed in the TIIS coordinate system.

Figure 7 shows a global overview of Titan's induced magnetosphere. It represents the projection of Cassini trajectories in dashed lines in the YZ plane of the DRAP, or TIIS, coordinate system depending on the possibility to determine the average upstream magnetic field. Curved trajectories are due to the temporal changes of the draped reference frame. In this coordinate system the upstream magnetic field direction points in the $-Z_{DRAP}$ direction while the convective electric field is directed along the $-Y_{DRAP}$ axis.

The bi-polarity of Titan's induced magnetosphere is emphasized with a clear reversal of the B_x component of the magnetic field indicating two magnetic lobe structures formed by the interaction of the moon ionosphere and the kronian plasma. The local B_x component is plotted along the DRAP/TIIS trajectory where the electron density is larger than 1 cm^{-3}. This result is compliant with the magnetotail structure characterized by Simon et al. (2010). Although the average magnetospheric field $< B_x >$ value has been substracted in order to remove a possible displacement of the neutral sheet due to the respective location of Titan with respect to Saturn's magnetodisk, the B_x reversal is not centered in the $Z = 0$ plane but may vary from flyby to flyby. It might be due to a North-South asymmetry of the magnetospheric flow or to a violation of the simplifying assumption that the magnetospheric field vary linearly between inbound and outbound magnetic field values, leading to an inaccurate estimate of the DRAP coordinate system.

Observed pick-up ion locations are displayed with filled circles (DRAP coordinate system) or squares (TIIS coordinate system) and the green-yellow color code indicates the energy. When the mass composition could be inferred, the symbol is surrounded by a red circle. All pick-up ions signatures found are localized in the $+E$ hemisphere, as expected from test-particle and global simulations (e.g., Luhmann, 1996; Modolo & Chanteur, 2008). Pickup ions with the lowest energy are observed preferentially in a range of Z_{DRAP} values between $\pm$ 2 R_T. Pickup ions with or without their mass composition present similar characteristics in term of position and energy. A progressive energization is clearly demonstrated by these Figures since pick-up ions observed farther from Titna reach higher energies up to several keV. Pickup gyroradius for ions of $m/q = 16$ and 28 in a typical kronian plasma at Titan's orbit is ~ 2 R$_T$ and ~ 3.5 R$_T$, respectively. Comparing these gyroradii with the pickup location in Figure 7 we can conclude that CAPS captured these pickup ions during their first gyration.

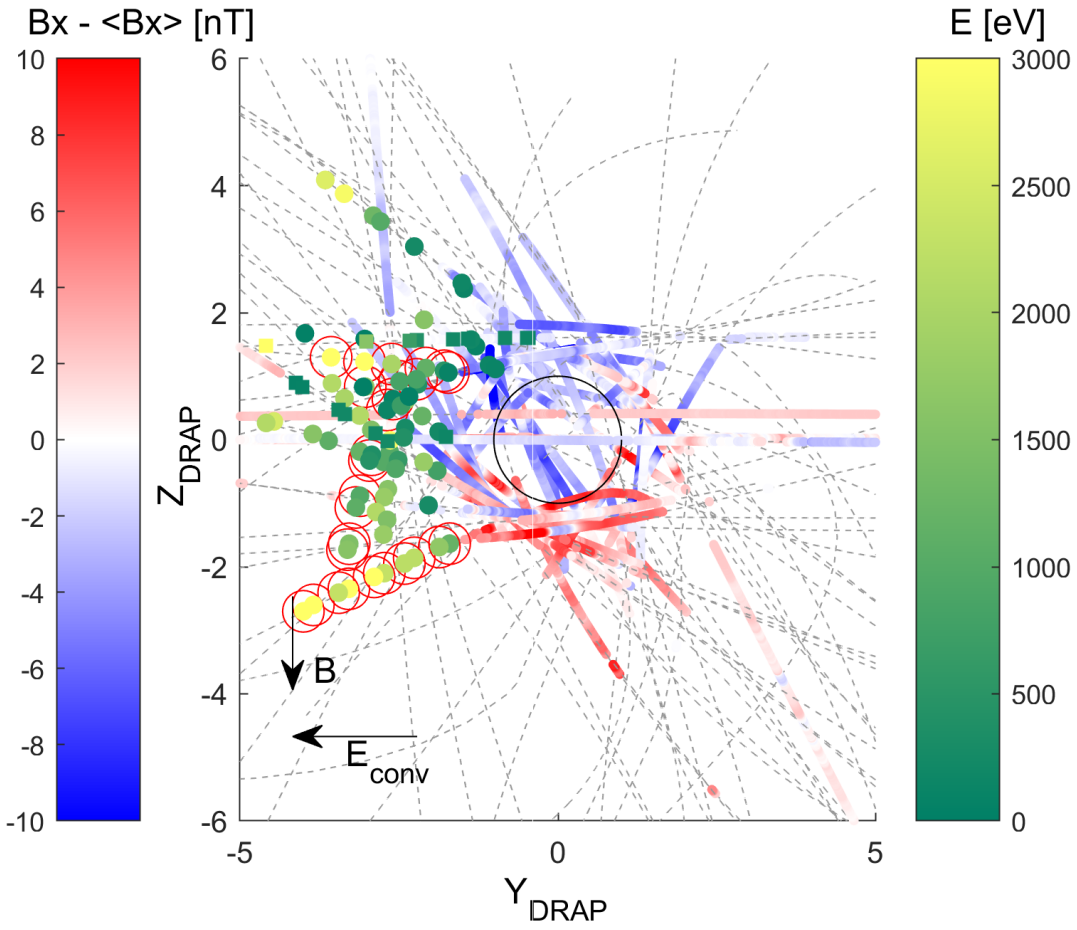

Figure 7. Projection of the Cassini flyby in the YZ_{DRAP} plane. Cassini's trajectories, in the DRAP coordinates, are shown by the dashed lines. Along the trajectory, the $B_x - < B_x >_{upstream}$ are colored, in blue-red colorbar, only in the induced magnetosphere region ($n_e > 1cm^{-3}$) and it emphasizes the two magnetic lobe polarities due to the draping. Filled dots and square symbols represent the pickup location in the DRAP and in the TIIS coordinates (when the upstream magnetic field could not be computed). The color code green-yellow colorbar, represent the energy in eV of the pickup ions. Filled dots with a red circle indicate the pickup ion when the mass composition could be determined.

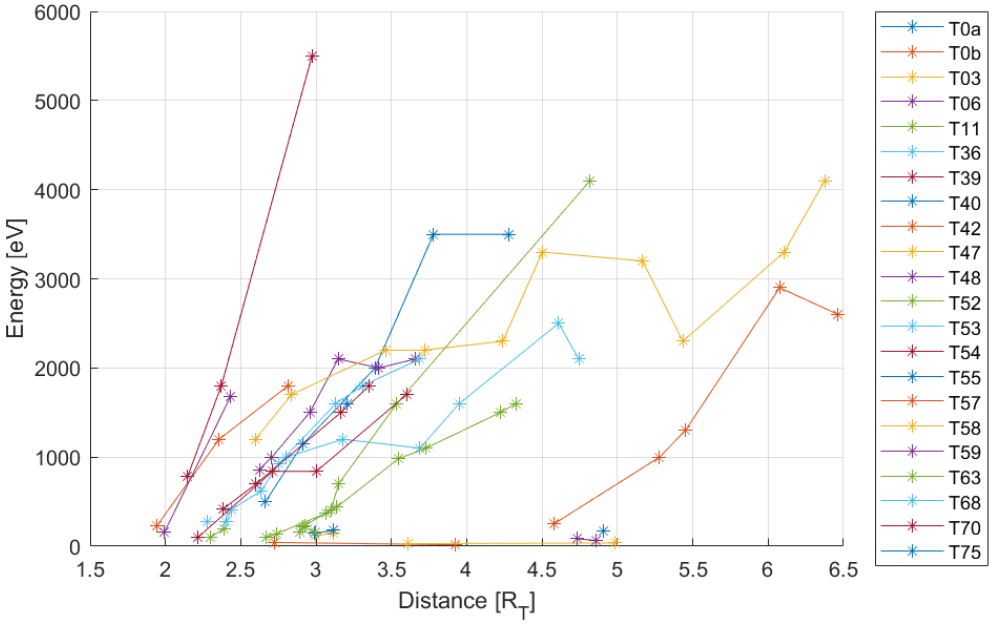

Figure 8. Pickup ion energy (in eV) in function of the distance to Titan (in R_T) for the different flybys where pickups ion have been identified.

Figure 8 displays the energy of the pickup ions as a function of the distance for flybys with pickup ion signatures. A clear linear relationship between the distance to the moon and the energy (up to 5.5 keV) is observed for a large majority of flybys. Assuming that the electric field is constant during a flyby outside of the induced magnetosphere, and integrating the equation of motion of a charged particle in a uniform electric field we can show that the energy gain of the particle depends on the electric field and the distance of acceleration ($\mathcal{E} = qE_{\perp}x$, with x the distance). A linear regression analysis for each flybys, having at least three pickup ion energy signatures, therefore provides an estimate of the intensity of the perpendicular component of the kronian electric field. We found that the kronian electric field varies between 0.22 mV/m and 2.24 mV/m, depending of the flybys. Averaging over all selected flybys, the kronian electric field is $E_{\perp} \simeq$ 0.70 mV/m. According to Wilson et al. (2017) the plasma velocity at 20 Saturn radii varies between $\sim$ 50 km/s and $\sim$ 200 km/s. The background magnetic field at Titan's orbit ranges from $\sim$ 2 nT to $\sim$ 6.5 nT with an average value of 4.4 nT, estimated from Table 1. With a typical velocity of 140 km/s along the corotation direction and an average magnetic field of 4.4 nT aligned with the Z_{TIIS} axis , the electric field is $E_{theo} =$

505 $|\vec{v} \times \vec{B}| \simeq 0.61$ mV/m in very good agreement with the elecric field intensity estimate
506 derived from pick-up ions.

507 5 Conclusions

508 Magnetometer data from MAG, particle data from CAPS and waves observations
509 from RPWS have been combined to present a global picture of Titan's induced magne-
510 tosphere and its pickup ion population.

511 Data from the CAPS-ELS electron spectrometer together with plasma wave ob-
512 servations from RPWS have provided for the whole set of flybys, from T0a to T82, con-
513 tinuous electron density profile ranging from 10^{-2} to several 10^3 ions.cm^{-3}. These pro-
514 files have been used to infer a global electron density map of Titan's near environment.

515 The cold ionsopheric plasma is confined on the ram-side below ~ 1.85 R_T to ~ 2.77
516 R_T, while it has been observed to extend farther than 6 Titan radii in the wake region.
517 The denser part of the induced magnetosphere is located in the ionosphere as expected,
518 while an extended plasma wake is reported. Although other factors, such as plasma beta,
519 local time and seasonal effects are expected to affect Titan's ionized environment, the
520 draping coordinate system proposed in this paper emphasizes the organization of Titan's
521 induced magnetosphere with respect to the kronian magnetic field. In the plane perpen-
522 dicular to the ideal corotational flow, an elliptical envelope elongated along the ambi-
523 ent field direction contains the cold plasma, supported by a clear evidence of bipolar mag-
524 netotail geometry. It can be used to determine an upper limit of a cross-section tail area,
525 required to compute total plasma loss rates.

526 Upstream of the induced magnetosphere, detection of pickup ions have been ob-
527 served and characterized with the ion mass spectrometer onboard Cassini spacecraft. The
528 mass composition of these pickups ions was determined in a few cases and time of flight
529 measurements have indicated the presence of methane group ions, molecular nitrogen
530 or $HCNH^+$ ions and lighter species such as protons and molecular hydrogen ions. These
531 pickup ions have been reported on the $+E$ hemisphere, close to the magnetic equator,
532 supporting theoretical or modelling results. A progressive energization is also observed,
533 and pickup ions with few keV have been identified as close as ~ 2 Titan radii. From their
534 energy signatures, the background electric field intensity is retrieved. Its value varies be-
535 tween 0.22 mV/m and 2.24 mV/m, with an average value of $\simeq 0.70$ mV/m in agreement

with a typical electric field assuming a plasma flow of 140 km/s and a magnetic field of 4.4 nT reported by recent studies.

Table 1: Titan flyby information. The first column indicates the reference number, the time of the closest approach and the Saturn location are reported in the second and third columns. The average background magnetic field, inbound and outbound are presented in he fourth and fifth column while the last two columns mark the presence of pickup ions by their energy signature and their mass composition respectively.

Flyby	Time (CA)	SLT [h]	B_{TIIS} [nT] Inbound	B_{TIIS} [nT] Outbound	Pick-up (Energy signature)	Pick-up (ion mass composition)
TA	2004-10-26T15:30:00.0	10.6	(0.4,2.6,-6.1)	(0.5, 2.7, -4.6)	x	N^+/CH_2^+, CH_4^+, $HCNH^+$ Hartle et al. (2006)
TB	2004-12-13T11:27:29.0	10.5	(0.9,3.8,-3.2)	(0.5,2.7,-4.6)	x	-
T03	2005-02-15T06:54:21.0	10.3	(1.4,3.6,-4.2)	(1.8,3.7,-4.00)	x	-
T05	2005-04-16T19:05:57.0	5.3	(1.7, 6.2, -4.7)	(2.4, 5.2, -4.1)		
T06	2005-08-22T18:54:50.0	5.0	(1.5,2.4,-1.1)	(0.3,3.5,-2.3)	x	-
T08	2005-10-28T03:58:09.0	9.3	(1.4,3.1,-2.4)	(1.9,4.1,-1.8)	-	-
T10	2006-01-15T11:36:46.0	8.5	(2.6,3.7,-3.5)	(3.0,3.6,-3.1)	-	-

T11	2006-02-27T08:20:44.0	1.1	(1.4,2.5,-2.9)	(0.1,3.9,-2.6)	x	-
T12	2006-03-12T23:58:17.0	6.4	(1.7,5.0,-2.9)	(3.3,5.6,-2.5)	-	-
T13	2006-04-30T20:53:31.0	23.2	(1.81,1.28,0.97)	(0.69,2.66,-2.46)	-	-
T14	2006-05-20T12:13:05.0	4.4	(0.9,4.4,-2.1)	(2.2,4.8,-2.1)	-	-
T15	2006-07-02T09:12:19.0	21.2	(2.1,3.6,-1.4)	(0.8,3.8,-2.3)	-	-
T16	2006-07-21T00:25:13.0	2.4	(-0.1,-1.5,-3.4)	(1.7,1.0,-2.4)	-	-
T17	2006-09-07T20:12:04	2.3	(0.0,2.8,-2.3)	(2.2,4.0,-1.4)	-	-
T18	2006-09-23T18:52:44.0	2.3	(1.8,5.0,-0.8)	(2.2,4.6,-1.1)	-	-
T19	2006-10-09T17:23:24.0	2.2	(-4.2,1.7,4.0)	(-0.6,2.6,-6.0)	-	-
T20	2006-10-25T15:51:29.0	2.2	(2.2,4.6,0.5)	(3.6,5.1,-0.4)	-	-
T21	2006-12-12T11:35:17.0	2.1	(3.3, 4.8, -1.4)	(2.8, 5.4, -1.2)	-	-
T22	2006-12-28T10:00:13.0	1.9	(2.1, 4.3, -1.7)	(0.6, 3.7, -2.1)	-	-
T23	2007-01-13T08:34:00.0	2.0	(3.0,5.3, -0.9)	-	-	-
T24	2007-01-29T07:12:10.0	1.9	(2.2, 4.4, -0.7)	(2.6, 4.7, -0.8)	-	-
T25	2007-02-22T03:10:59.0	13.9	(0.2, -0.2, -2.8)	-	-	-
T26	2007-03-10T01:47:22	13.8	(2.3, 1.8, -2.7)	(0.8, 2.9, -2.5)	-	-
T27	2007-03-25T00:21:52.0	13.8	(0.6, 1.2, -2.0)	(-0.4, 0.6, -2.7)	-	-
T28	2007-04-10T22:57:11.0	13.7	(-0.8, 0.0, -6.2)	(0.8, 1.5, -5.2)	-	-

T29	2007-04-26T21:32:52.0	13.7	(-0.4, 1.8, -3.9)	(-1.9, 2.4, -6.4)	-	-
T30	2007-02-12T20:08:14.0	13.6	(-0.4, 2.3, -4.1)	(-2.1, 0.3, -4.0)	-	-
T31	2007-05-28T18:51:27.0	13.6	(0.3, 1.5, -3.5)	-	-	-
T33	2007-06-29T17:05:01.0	13.6	(-1.9, 2.2, -4.2)	(-0.9, 3.4, -5.3)	-	-
T34	2007-07-18T00:41:02.0	18.8	(-1.6, 2.3, -1.8)	(0.4, 2.1, -2.5)	-	-
T35	2007-08-31T06:34:25.0	11.5	(1.0, 3.0, -1.2)	-	-	-
T36	2007-10-02T04:49:50.0	11.5	(2.3, 1.9, -5.3)	(1.3, 0.7, -3.3)	x	CH_2^+, CH_3^+, CH_4^+, H_2CN^+, H^+, H_2^+
T37	2007-11-19T00:52:51.0	11.4	(0.7, 2.3, -1.6)	-	-	-
T38	2007-12-04T00:07:37.0	11.4	(3.0, 1.8, -4.4)	(1.1, 0.8, -6.0)	-	-
T39	2007-12-20T22:56:41.0	11.4	(-0.2, 1.1, -9.1)	-	x	-
T40	2008-01-05T21:26:24.0	11.3	(-0.5, 2.0, -1.9)	-	x	-
T41	2008-02-22T17:39:23.0	11.2	(1.2, 3.5, -2.5)	-	-	-
T42	2008-03-25T14:36:12.0	11.1	(-0.4, 0.7, -8.0)	-	-	-
T43	2008-05-12T10:09:59.0	11.0	(0.6, 0.4, -4.0)	(-0.3, 2.7, -3.4)	-	-
T44	2008-05-28T08:33:21.0	10.9	(0.3, 0.4, -5.5)	(-0.6, 0.5, -7.2)	-	-
T45	2008-07-31T02:13:11.0	10.7	(1.6, 3.3, -2.1)	-	-	-
T46	2008-11-03T17:35:23.0	10.5	(1.8, 2.0, -0.7)	(-0.1, 1.6, -1.2)	-	-
T47	2008-11-19T15:56:28.0	10.4	(0.9, 0.7, -1.6)	(-0.4, -1.0, -1.6)	x	CH_2^+, CH_3^+, CH_4^+, H^+, H_2^+

T48	2008-12-05T14:25:45	10.4	(1.3, 2.8, -1.3)	(-0.4, 1.0, -1.5)	x	-
T49	2008-12-21T12:59:53	10.3	(2.3, 3.8, -3.1)	(0.7, 3.2, -2.7)	-	-
T50	2008-02-07T08:50:51	10.2	(2.9, -0.2, -1.7)	(0.9, 0.3, -2.7)	-	-
T51	2009-03-27T04:43:36	10.1	(1.2, 3.1, -1.4)	(0.5, 0.3, -3.8)	-	-
T52	2009-04-04T01:47:47	22.1	(1.3, 3.1, -1.4)	(0.5, 0.4, -3.9)	x	CH_3^+, CH_4^+, H_2CN^+, N_2^+, H_2^+, H^+
T53	2009-04-20T00:20:45	22.1	(0.2, -0.3, -3.2)	(1.5, 1.7, -2.4)	x	
T54	2009-05-05T18:32:35	22.0	(1.9, 4.3, -0.9)	(-1.5, -2.2, -0.9)	-	
T55	2009-05-21T21:26:41	22.0	(0.1, 1.4, -0.9)	(1.3, 3.6, -1.4)	x	-
T56	2009-06-06T20:00:00	21.9	(0.7, 5.4, -1.7)	(-2.9, -1.3, -1.5)	-	-
T57	2009-06-22T18:32:35	21.9	(0.9, 0.8, -2.3)	(2.5, 4.0, -1.6)	x	-
T58	2009-07-08T17:05:009	21.8	(2.0, 4.1, 0.5)	(-0.3, 2.0, -1.8)	x	-
T59	2009-07-24T15:35:09	21.8	-	-	x (TIIS)	CH_3^+, CH_4^+, CH_5^+, H_2CN^+, H_2^+, H^+
T61	2009-08-25T12:52:44	21.7	-	-	-	-
T62	2009-10-12T08:37:30	21.6	-	-	-	-
T63	2009-12-12T01:04:20	17.0	-	-	x (TIIS)	-
T64	2009-12-28T00:18:05	16.8	(-1.7, -1.5, -1.5)	(-0.9, -1.9, -1.7)	-	-
T65	2010-01-12T23:11:42	16.9	(0.2, 3.0, -4.8)	(-0.6, -2.5, -1.6)	-	-
T66	2010-01-28T22:29:55	21.0	-	-	-	-

T67	2010-04-05T15:51:44	16.1	-	-	-	-
T68	2010-05-20T03:25:26	16.0	(1.5, 1.9, -1.8)	(-1.1, -1.7, -1.5)	x	-
T69	2010-06-05T02:27:33	16.0	(0.5, -1.2, -3.3)	(1.5, 1.8, -2.6)	-	-
T70	2010-06-21T01:28:23	16.1	(0.1, -0.8, -4.6)	(0.1, -0.1, -5.9)	x	CH_4^+, CH_3^+, H_2CN^+, H^+, H_2^+, CH_5^+, H_2O^+
T71	2010-07-07T00:22:35	16.1	(0.3, -0.5, -2.7)	(0.7, 0.4, -2.7)	-	-
T72	2010-09-24T18:38:41	15.9	-	-	-	-
T74	2011-02-08T16:04:11	20.6	-	-	-	-
T75	2011-04-19T05:00:39	14.2	-	-	x (TIIS)	-
T76	2011-05-08T22:53:44	19.8	-	-	-	-
T77	2011-06-20T18:32:01	12.2	(0.3, -1.4, -4.3)	(0.0, -1.4, -5.1)	-	-
T78	2011-09-12T02:50:05	17.5	(0.3, 1.9, -2.7)	(-1.8, -2.3, -2.2)	-	-
T82	2012-02-19T08:43:17	18.3	-	-	-	-

Acknowledgments

RM, JJB, PC, RP and FL are indebted to the "Soleil, Heliosphere, Magnetosphere" group of CNES for its support. It is based on observations with RPWS, CAPS, MAG embarked on Cassini. The Cassini data used in this paper are available at the NASA Planetary Data System (`https://pds-ppi.igpp.ucla.edu`). The authors are grateful to the French "Centre de Données sur la Physique des Plasmas" for the access to the visualization tools AMDA.

References

Ågren, K., Wahlund, J., Garnier, P., Modolo, R., Cui, J., Galand, M., & Müller-Wodarg, I. (2009, December). On the ionospheric structure of Titan. *Planet. Space Sci.*, *57*, 1821-1827. doi: 10.1016/j.pss.2009.04.012

Arridge, C. S. (2012). A statistical analysis of plasma parameters near Titan's orbit. *J. Geophys. Res.*.

Arridge, C. S., Achilleos, N., & Guio, P. (2011, July). Electric field variability and classifications of Titan's magnetoplasma environment. *Annales Geophysicae*, *29*, 1253-1258. doi: 10.5194/angeo-29-1253-2011

Arridge, C. S., André, N., Bertucci, C. L., Garnier, P., Jackman, C. M., Németh, Z., ... Crary, F. J. (2011, December). Upstream of Saturn and Titan. , *162*, 25-83. doi: 10.1007/s11214-011-9849-x

Arridge, C. S., André, N., McAndrews, H. J., Bunce, E. J., Burger, M. H., Hansen, K. C., ... Dougherty, M. K. (2011, December). Mapping Magnetospheric Equatorial Regions at Saturn from Cassini Prime Mission Observations. , *164*, 1-83. doi: 10.1007/s11214-011-9850-4

Barabash, S. (2012, February). Classes of the solar wind interactions in the solar system. *Earth, Planets, and Space*, *64*(2), 57-59. doi: 10.5047/eps.2012.01.005

Bertucci, C., Achilleos, N., Dougherty, M. K., Modolo, R., Coates, A. J., Szego, K., ... Young, D. T. (2008, September). The Magnetic Memory of Titan's Ionized Atmosphere. *Science*, *321*, 1475-. doi: 10.1126/science.1159780

Bertucci, C., Duru, F., Edberg, N., Fraenz, M., Martinecz, C., Szego, K., & Vaisberg, O. (2011, December). The Induced Magnetospheres of Mars, Venus, and Titan. , *162*(1-4), 113-171. doi: 10.1007/s11214-011-9845-1

Bertucci, C., Sinclair, B., Achilleos, N., Hunt, P., Dougherty, M. K., & Arridge, C. S. (2009, December). The variability of Titan's magnetic environment. *Planet. Space Sci.*, *57*, 1813-1820. doi: 10.1016/j.pss.2009.02.009

Chen, C., & Simon, S. (2020). A comprehensive study of titan's magnetic pile-up region during the cassini era. *Planetary and Space Science*, *191*, 105037. Retrieved from `http://www.sciencedirect.com/science/article/pii/S0032063319305392` doi: https://doi.org/10.1016/j.pss.2020.105037

Coates, A. J. (2009, February). Interaction of Titan's ionosphere with Saturn's magnetosphere. *Royal Society of London Philosophical Transactions Series A*, *367*, 773-788. doi: 10.1098/rsta.2008.0248

Coates, A. J., Crary, F. J., Young, D. T., Szego, K., Arridge, C. S., Bebesi, Z., ... Hill, T. W. (2007). Ionospheric electrons in titan's tail: Plasma structure during the cassini t9 encounter. *Geophysical Research Letters*, *34*(24). Retrieved from `https://agupubs.onlinelibrary.wiley.com/doi/abs/10.1029/2007GL030919` doi: 10.1029/2007GL030919

Coates, A. J., Johnstone, A. D., Huddleston, D. E., Wilken, B., Jockers, K., Borg, H., ... Neubauer, F. M. (1993, March). Pickup water group ions at Comet Grigg-Skjellerup. *Geophys. Res. Lett.*, *20*, 483-486. doi: 10.1029/93GL00174

Coates, A. J., Johnstone, A. D., Wilken, B., Jockers, K., & Glassmeier, K.-H. (1989, August). Velocity space diffusion of pickup ions from the water group at Comet Halley. *J. Geophys. Res.*, *94*, 9983-9993. doi: 10.1029/JA094iA08p09983

Coates, A. J., Wellbrock, A., Lewis, G. R., Arridge, C. S., Crary, F. J., Young, D. T., ... Jones, G. H. (2012). Cassini in titan's tail: Caps observations of plasma escape. *Journal of Geophysical Research: Space Physics*, *117*(A5). Retrieved from `https://agupubs.onlinelibrary.wiley.com/doi/abs/10.1029/2012JA017595` doi: 10.1029/2012JA017595

Cowee, M. M., Gary, S. P., Wei, H. Y., Tokar, R. L., & Russell, C. T. (2010). An explanation for the lack of ion cyclotron wave generation by pickup ions at titan: 1-d hybrid simulation results. *Journal of Geophysical Research: Space Physics*, *115*(A10). Retrieved from `https://agupubs.onlinelibrary.wiley.com/doi/abs/10.1029/2010JA015769` doi: 10.1029/2010JA015769

Cravens, T. E., Yelle, R. V., Wahlund, J.-E., Shemansky, D. E., & Nagy, A. F.

(2010). Composition and Structure of the Ionosphere and Thermosphere. In R. H. Brown, J.-P. Lebreton, & J. H. Waite (Eds.), *Titan from cassini-huygens* (p. 259). doi: 10.1007/978-1-4020-9215-2-11

Delva, M., Mazelle, C., & Bertucci, C. (2012). Upstream Ion Cyclotron Waves at Venus and Mars. In *The plasma environment of venus* (Vol. 37, p. 5). doi: 10.1007/s11214-011-9828-2

Dougherty, M. K., Kellock, S., Southwood, D. J., Balogh, A., Smith, E. J., Tsurutani, B. T., ... Cowley, S. W. H. (2004, September). The Cassini Magnetic Field Investigation. *Space Science Reviews*, *114*, 331-383. doi: 10.1007/s11214-004-1432-2

Dubinin, E., Fraenz, M., Woch, J., Barabash, S., Lundin, R., & Yamauchi, M. (2006, November). Hydrogen exosphere at Mars: Pickup protons and their acceleration at the bow shock. *Geophys. Res. Lett.*, *33*, 22103. doi: 10.1029/2006GL027799

Dubinin, E., Lundin, R., Koskinen, H., & Norberg, O. (1993, April). Cold ions at the Martian bow shock - PHOBOS observations. *J. Geophys. Res.*, *98*, 5617-5623. doi: 10.1029/92JA02374

Dubinin, E., Modolo, R., Fraenz, M., Päetzold, M., Woch, J., Chai, L., ... Zelenyi, L. (2019). The induced magnetosphere of mars: Asymmetrical topology of the magnetic field lines. *Geophysical Research Letters*, *46*(22), 12722-12730. Retrieved from `https://agupubs.onlinelibrary.wiley.com/doi/abs/10.1029/2019GL084387` doi: 10.1029/2019GL084387

Edberg, N., Ågren, K., Wahlund, J.-E., Morooka, M., Andrews, D., Cowley, S., ... Dougherty, M. (2011). Structured ionospheric outflow during the cassini t55–t59 titan flybys. *Planetary and Space Science*, *59*(8), 788 - 797. Retrieved from `http://www.sciencedirect.com/science/article/pii/S0032063311000948` doi: https://doi.org/10.1016/j.pss.2011.03.007

Edberg, N. J. T., Andrews, D. J., Bertucci, C., Gurnett, D. A., Holmberg, M. K. G., Jackman, C. M., ... Wahlund, J.-E. (2015). Effects of saturn's magnetospheric dynamics on titan's ionosphere. *Journal of Geophysical Research: Space Physics*, *120*(10), 8884-8898. Retrieved from `https://agupubs.onlinelibrary.wiley.com/doi/abs/10.1002/2015JA021373` doi: 10.1002/2015JA021373

Edberg, N. J. T., Andrews, D. J., Shebanits, O., Ågren, K., Wahlund, J., Opgenoorth, H. J., ... Girazian, Z. (2013). Solar cycle modulation of titan's ionosphere. *Journal of Geophysical Research: Space Physics*, *118*(8), 5255-5264. Retrieved from `https://agupubs.onlinelibrary.wiley.com/doi/abs/10.1002/jgra.50463` doi: 10.1002/jgra.50463

Edberg, N. J. T., Wahlund, J.-E., Ågren, K., Morooka, M. W., Modolo, R., Bertucci, C., & Dougherty, M. K. (2010, October). Electron density and temperature measurements in the cold plasma environment of Titan: Implications for atmospheric escape. *Geophys. Res. Lett.*, *37*, 20105. doi: 10.1029/2010GL044544

Felici, M., Arridge, C. S., Wilson, R. J., Coates, A. J., Thomsen, M., & Reisenfeld, D. (2018). Survey of thermal plasma composition in saturn's magnetosphere using time-of-flight data from cassini/caps. *Journal of Geophysical Research: Space Physics*, *123*(8), 6494-6513. Retrieved from `https://agupubs.onlinelibrary.wiley.com/doi/abs/10.1029/2017JA025085` doi: 10.1029/2017JA025085

Garnier, P., Dandouras, I., Toublanc, D., Roelof, E. C., Brandt, P. C., Mitchell, D. G., ... Wahlund, J.-E. (2010, December). Statistical analysis of the energetic ion and ENA data for the Titan environment. *Planet. Space Sci.*, *58*, 1811-1822. doi: 10.1016/j.pss.2010.08.009

Gurnett, D. A., Kurth, W. S., Kirchner, D. L., Hospodarsky, G. B., Averkamp, T. F., Zarka, P., ... Pedersen, A. (2004, September). The Cassini Radio and Plasma Wave Investigation. *Space Science Reviews*, *114*, 395-463. doi: 10.1007/s11214-004-1434-0

Halekas, J. S., Brain, D. A., Luhmann, J. G., DiBraccio, G. A., Ruhunusiri, S., Harada, Y., ... Jakosky, B. M. (2017). Flows, fields, and forces in the mars-solar wind interaction. *Journal of Geophysical Research: Space Physics*, *122*(11), 11,320-11,341. Retrieved from `https://agupubs.onlinelibrary.wiley.com/doi/abs/10.1002/2017JA024772` doi: 10.1002/2017JA024772

Hartle, R. E., Sarantos, M., & Sittler, E. C., Jr. (2011, October). Pickup ion distributions from three-dimensional neutral exospheres. *Journal of Geophysical Research (Space Physics)*, *116*(A15), 10101. doi: 10.1029/2011JA016859

Hartle, R. E., & Sittler, E. C. (2007, July). Pickup ion phase space distributions: Effects of atmospheric spatial gradients. *Journal of Geophysical Research (Space*

Physics), *112*, 7104. doi: 10.1029/2006JA012157

Hartle, R. E., Sittler, E. C., Neubauer, F. M., Johnson, R. E., Smith, H. T., Crary, F., ... Andre, N. (2006, April). Preliminary interpretation of Titan plasma interaction as observed by the Cassini Plasma Spectrometer: Comparisons with Voyager 1. *Geophys. Res. Lett.*, *33*, 8201-+. doi: 10.1029/2005GL024817

Hartle, R. E., Sittler, E. C., Ogilvie, K. W., Scudder, J. D., Lazarus, A. J., & Atreya, S. K. (1982, March). Titan's ion exosphere observed from Voyager 1. *J. Geophys. Res.*, *87*, 1383-1394. doi: 10.1029/JA087iA03p01383

Ledvina, S. A., Brecht, S. H., & Cravens, T. E. (2012, February). The orientation of Titan's dayside ionosphere and its effects on Titan's plasma interaction. *Earth, Planets, and Space*, *64*, 207-230. doi: 10.5047/eps.2011.08.009

Lewis, G. R., André, N., Arridge, C. S., Coates, A. J., Gilbert, L. K., Linder, D. R., & Rymer, A. M. (2008, May). Derivation of density and temperature from the Cassini Huygens CAPS electron spectrometer. *Planet. Space Sci.*, *56*, 901-912. doi: 10.1016/j.pss.2007.12.017

Luhmann, J. G. (1996). Titan's ion exosphere wake: A natural ion mass spectrometer? *Journal of Geophysical Research: Planets*, *101*(E12), 29387-29393. Retrieved from `https://agupubs.onlinelibrary.wiley.com/doi/abs/10.1029/96JE03307` doi: 10.1029/96JE03307

Ma, Y., Nagy, A. F., Cravens, T. E., Sokolov, I. V., Hansen, K. C., Wahlund, J.-E., ... Dougherty, M. K. (2006, May). Comparisons between MHD model calculations and observations of Cassini flybys of Titan. *Journal of Geophysical Research (Space Physics)*, *111*, 5207. doi: 10.1029/2005JA011481

Modolo, R., & Chanteur, G. M. (2008, January). A global hybrid model for Titan's interaction with the Kronian plasma: Application to the Cassini Ta flyby. *J. Geophys. Res.*, *113*(A12), 1317-+. doi: 10.1029/2007JA012453

Modolo, R., Chanteur, G. M., Wahlund, J.-E., Canu, P., Kurth, W. S., Gurnett, D., ... Bertucci, C. (2007). Plasma environment in the wake of titan from hybrid simulation: A case study. *Geophysical Research Letters*, *34*(24). Retrieved from `https://agupubs.onlinelibrary.wiley.com/doi/abs/10.1029/2007GL030489` doi: 10.1029/2007GL030489

Modolo, R., Wahlund, J., Boström, R., Canu, P., Kurth, W. S., Gurnett, D., ... Coates, A. J. (2007, October). Far plasma wake of Titan from the

RPWS observations: A case study. *Geophys. Res. Lett.*, *34*, 24-+. doi: 10.1029/2007GL030482

Morooka, M., Modolo, R., Wahlund, J. E., André, M., Eriksson, A. I., Persoon, D. A., A. M. andGurnett, ... Dougherty, M. (2009). The electron density of Saturn's magnetosphere. *Annales Geophysicae*, *27*, 2971-2991. doi: 10.5194/angeo-27-2971-2009

Nelson, D., & Berthelier, J. J. (2009). *Caps simulator, handbook* (Tech. Rep.). LATMOS.

Neubauer, F. M., Backes, H., Dougherty, M. K., Wennmacher, A., Russell, C. T., Coates, A., ... Saur, J. (2006, October). Titan's near magnetotail from magnetic field and electron plasma observations and modeling: Cassini flybys TA, TB, and T3. *J. Geophys. Res.*, *111*(A10), 10220-+. doi: 10.1029/2006JA011676

Németh, Z., Szego, K., Bebesi, Z., Erdős, G., Foldy, L., Rymer, A., ... Wellbrock, A. (2011). Ion distributions of different kronian plasma regions. *Journal of Geophysical Research: Space Physics*, *116*(A9). Retrieved from `https://agupubs.onlinelibrary.wiley.com/doi/abs/10.1029/2011JA016585` doi: 10.1029/2011JA016585

Regoli, L. H., Coates, A. J., Thomsen, M. F., Jones, G. H., Roussos, E., Waite, J. H., ... Cox, G. (2016, September). Survey of pickup ion signatures in the vicinity of Titan using CAPS/IMS. *Journal of Geophysical Research (Space Physics)*, *121*, 8317-8328. doi: 10.1002/2016JA022617

Regoli, L. H., Roussos, E., Dialynas, K., Luhmann, J. G., Sergis, N., Jia, X., ... Rae, I. J. (2018). Statistical study of the energetic proton environment at titan's orbit from the cassini spacecraft. *Journal of Geophysical Research: Space Physics*, *123*(6), 4820-4834. Retrieved from `https://agupubs.onlinelibrary.wiley.com/doi/abs/10.1029/2018JA025442` doi: 10.1029/2018JA025442

Romanelli, N., Bertucci, C., Gómez, D., Mazelle, C., & Delva, M. (2013, February). Proton cyclotron waves upstream from Mars: Observations from Mars Global Surveyor. *Planet. Space Sci.*, *76*, 1-9. doi: 10.1016/j.pss.2012.10.011

Romanelli, N., Modolo, R., Dubinin, E., Berthelier, J.-J., Bertucci, C., Wahlund, J. E., ... Dougherty, M. (2014). Outflow and plasma acceleration in titan's

induced magnetotail: Evidence of magnetic tension forces. *Journal of Geophysical Research: Space Physics*, *119*(12), 9992-10,005. Retrieved from https://agupubs.onlinelibrary.wiley.com/doi/abs/10.1002/2014JA020391 doi: 10.1002/2014JA020391

Russell, C. T., Wei, H. Y., Cowee, M. M., Neubauer, F. M., & Dougherty, M. K. (2016). Ion cyclotron waves at titan. *Journal of Geophysical Research: Space Physics*, *121*(3), 2095-2103. Retrieved from https://agupubs.onlinelibrary.wiley.com/doi/abs/10.1002/2015JA022293 doi: 10.1002/2015JA022293

Rymer, A. M., Smith, H. T., Wellbrock, A., Coates, A. J., & Young, D. T. (2009, August). Discrete classification and electron energy spectra of Titan's varied magnetospheric environment. *Geophys. Res. Lett.*, *36*, 15109-+. doi: 10.1029/2009GL039427

Sillanpää, I., Kallio, E., Janhunen, P., Schmidt, W., Mursula, K., Vilppola, J., & Tanskanen, P. (2006). Hybrid simulation study of ion escape at Titan for different orbital positions. *Advances in Space Research*, *38*, 799-805. doi: 10.1016/j.asr.2006.01.005

Simon, S., Boesswetter, A., Bagdonat, T., Motschmann, U., & Schuele, J. (2007, February). Three-dimensional multispecies hybrid simulation of Titan's highly variable plasma environment. *Annales Geophysicae*, *25*, 117-144.

Simon, S., Neubauer, F. M., Wennmacher, A., & Dougherty, M. K. (2014, March). Variability of Titan's induced magnetotail: Cassini magnetometer observations. *Journal of Geophysical Research (Space Physics)*, *119*, 2024-2037. doi: 10.1002/2013JA019608

Simon, S., van Treeck, S. C., Wennmacher, A., Saur, J., Neubauer, F. M., Bertucci, C. L., & Dougherty, M. K. (2013). Structure of titan's induced magnetosphere under varying background magnetic field conditions: Survey of cassini magnetometer data from flybys ta–t85. *Journal of Geophysical Research: Space Physics*, *118*(4), 1679-1699. Retrieved from https://agupubs.onlinelibrary.wiley.com/doi/abs/10.1002/jgra.50096 doi: 10.1002/jgra.50096

Simon, S., Wennmacher, A., M., N., Bertucci, C. L., Kriegel, H., Saur, J., ... Dougherty, M. K. (2010). Titan's highly dynamicmagnetic environment : A systematic survey of cassini magnetometer observations from flybys ta-t62.

Planet. Space Sci.. doi: 10.1016/j.pss.2010.04.021

Sittler, E. C., Hartle, R. E., Johnson, R. E., Cooper, J. F., Lipatov, A. S., Bertucci, C., ... Wahlund, J.-E. (2010, February). Saturn's magnetospheric interaction with Titan as defined by Cassini encounters T9 and T18: New results. *Planet. Space Sci.*, *58*, 327-350. doi: 10.1016/j.pss.2009.09.017

Snowden, D., Winglee, R., Bertucci, C., & Dougherty, M. (2007, December). Three-dimensional multifluid simulation of the plasma interaction at Titan. *Journal of Geophysical Research (Space Physics)*, *112*(A11), 12221. doi: 10.1029/2007JA012393

Szego, K., Bebesi, Z., Bertucci, C., Coates, A. J., Crary, F., Erdos, G., ... Young, D. T. (2007, November). Charged particle environment of Titan during the T9 flyby. *Geophys. Res. Lett.*, *34*, 24-+. doi: 10.1029/2007GL030677

Thomsen, M. F., Reisenfeld, D. B., Delapp, D. M., Tokar, R. L., Young, D. T., Crary, F. J., ... Williams, J. D. (2010). Survey of ion plasma parameters in saturn's magnetosphere. *Journal of Geophysical Research: Space Physics*, *115*(A10). Retrieved from `https://agupubs.onlinelibrary.wiley.com/doi/abs/10.1029/2010JA015267` doi: 10.1029/2010JA015267

Thomsen, M. F., Reisenfeld, D. B., Wilson, R. J., Andriopoulou, M., Crary, F. J., Hospodarsky, G. B., ... Tokar, R. L. (2014). Ion composition in interchange injection events in saturn's magnetosphere. *Journal of Geophysical Research: Space Physics*, *119*(12), 9761-9772. Retrieved from `https://agupubs.onlinelibrary.wiley.com/doi/abs/10.1002/2014JA020489` doi: 10.1002/2014JA020489

Tokar, R. L., Wilson, R. J., Johnson, R. E., Henderson, M. G., Thomsen, M. F., Cowee, M. M., ... Smith, H. T. (2008, July). Cassini detection of water-group pick-up ions in the Enceladus torus. *Geophys. Res. Lett.*, *35*, 14202. doi: 10.1029/2008GL034749

Wahlund, J.-E., Boström, R., Gustafsson, G., Gurnett, D. A., Kurth, W. S., Pedersen, A., ... Müller-Wodarg, I. (2005, May). Cassini Measurements of Cold Plasma in the Ionosphere of Titan. *Science*, *308*, 986-989. doi: 10.1126/science.1109807

Wahlund, J.-E., Modolo, R., Bertucci, C., & Coates, A. (2014). Titan's Magnetospheric and Plasma Environment. In I. Müller-Wodarg, C. A. Griffith,

E. Lellouch, & T. E. Cravens (Eds.), *Titan: Surface, Atmosphere and Magnetosphere.* Cambridge University Press.

Waite, J. H., Lewis, W. S., Kasprzak, W. T., Anicich, V. G., Block, B. P., Cravens, T. E., ... Yelle, R. V. (2004, September). The Cassini Ion and Neutral Mass Spectrometer (INMS) Investigation. , *114*(1-4), 113-231. doi: 10.1007/s11214-004-1408-2

Westlake, J. H., Paranicas, C. P., Cravens, T. E., Luhmann, J. G., Mandt, K. E., Smith, H. T., ... Wahlund, J.-E. (2012). The observed composition of ions outflowing from titan. *Geophysical Research Letters*, *39*(19). Retrieved from `https://agupubs.onlinelibrary.wiley.com/doi/abs/10.1029/2012GL053079` doi: 10.1029/2012GL053079

Wilson, R. J., Bagenal, F., & Persoon, A. M. (2017). Survey of thermal plasma ions in saturn's magnetosphere utilizing a forward model. *Journal of Geophysical Research: Space Physics*, *122*(7), 7256-7278. Retrieved from `https://agupubs.onlinelibrary.wiley.com/doi/abs/10.1002/2017JA024117` doi: 10.1002/2017JA024117

Wilson, R. J., Crary, F., Gilbert, L. K., Reisenfeld, D. B., Steinberg, J. T., & Livi, R. (2012). Pds user's guide for cassini plasma spectrometer. *PDS*. Retrieved from `https://pds-ppi.igpp.ucla.edu/`

Yokota, S., Saito, Y., Asamura, K., Tanaka, T., Nishino, M. N., Tsunakawa, H., ... Terasawa, T. (2009, June). First direct detection of ions originating from the Moon by MAP-PACE IMA onboard SELENE (KAGUYA). *Geophys. Res. Lett.*, *36*, 11201. doi: 10.1029/2009GL038185

Young, D. T., Berthelier, J. J., Blanc, M., Burch, J. L., Coates, A. J., Goldstein, R., ... Zinsmeyer, C. (2004, September). Cassini Plasma Spectrometer Investigation. *Space Science Reviews*, *114*, 1-112. doi: 10.1007/s11214-004-1406-4